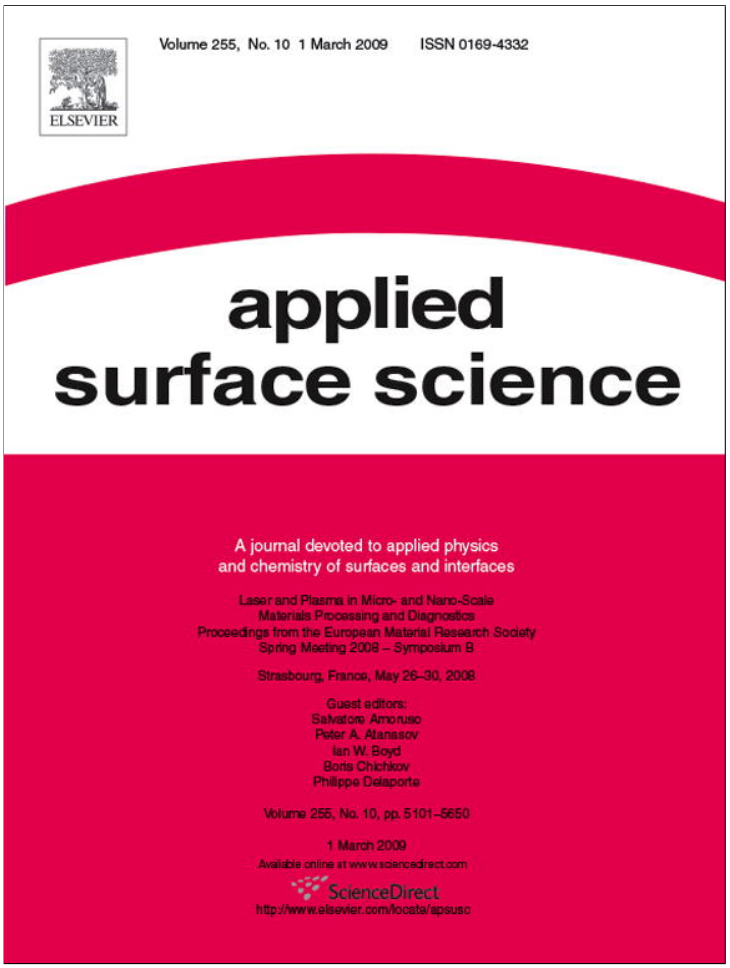

Applied Surface Science 255 (2009) 5112–5115

Contents lists available at ScienceDirect

Applied Surface Science

journal homepage: www.elsevier.com/locate/apsusc

Modeling of fast phase transitions dynamics in metal target irradiated by pico- and femtosecond pulsed laser

V.I. Mazhukin [a], M.G. Lobok [a,*], B. Chichkov [b]

[a] Institute of Mathematical Modeling, Russian Academy of Sciences, Miusskaya sq. 4A, 125047 Moscow, Russia
[b] Laser Zentrum Hannover e.V. Holleritallee 8, 30419 Hannover, Germany

ARTICLE INFO

Article history:
Available online 20 August 2008

Keywords:
Stephan problem
Rapid phase transitions
Overheating

ABSTRACT

We investigate laser pulse influence on aluminum target in irradiance range 10^9 to 10^{16} W/cm^2, pulse duration between 10^{-8} and 10^{-15} s, Gaussian time profile with wavelength of 0.8 μm. For all computations energy density was 10 J/cm^2. Plasma in the evaporated material is generated at the energy density above 10 J/cm^{2}as the modeling showed.

Long and short laser pulses distinguish by the mechanisms of energy transformation. For short laser pulses there is volumetric energy absorption, together with rapid phase transitions it lead to overheating in solid and liquid states, overheated solid temperature rises up to (6–8)T_m. Under influence of the energy saved in overheated solid, duration of the phase transitions becomes nanosecond, which is several orders of magnitude longer than laser pulse.

1. Introduction

Laser ablation is widely used in rapidly increasing quantity of applications [1]. Number of publications on ultra-short laser processing is steadily growing. The majority of them cover experimental observations [2–4] and only few of them seek to provide a theoretical basis for the fundamental phenomena [5–7] that accompany exposure to ultra-short laser pulses. To sum up the deliverables of experimental research [2] related to laser metal micromachining with ultra-short pulses, we should mention their peculiarities and advantages as follows:

- Shifting from nano- to femtosecond pulse duration liquid fraction share is being reduced and hole quality is improving. The average vaporized layer thickness with the value of $J < 1$ J/cm^2 does not exceed 100 nm, and grows as we increase J.
- There is no plasma formation occurrence in case of pico- and femtosecond duration with laser intensity of $J < 5$ J/cm^2.
- Heat conduction effects are negligible on impulse time scale.

The main features of the ultra-short laser pulse treatment of metals are associated with high velocity and volumetric character of energy liberation. High heating of the solid velocity is conjugated with rapid phase transformations of the matter, which are characterized by major mass and energy flux through the interphase boundaries. Energy flux caused by mass flow combined with volumetric laser pulse energy liberation leads to the overheating of the interphase boundaries up to the values that significantly greater than equilibrium temperatures of melting and evaporation. The same reasons result the occurrence of near surface maximums of the temperature in liquid and solid states.

Overheated metastable states, arising from laser treatment are investigated both experimentally [8–11] and theoretically [12–17]. This work is devoted to the investigation of the conditions metastable states formation and phase transformation dynamics in Al targets irradiated by pico- and femtosecond laser pulses.

2. Problem statement

Laser beam propagates from right to left side, partly reflexes from the surface (Fig. 1). Spatial distribution of phases, interphase boundaries and shockwaves are also shown in Fig. 1.

Problem statement has the following assumptions and limitations: laser energy is realized instantly for the lattice, phase transformations are thermal by its nature, and volumetric melting and evaporation are excluded. We assume that melting front appears when the surface temperature rises up to $T_{m,0}$. Overheated metastable states behave steady.

Mathematical formulation and modeling of laser ablation of solid aluminum target in counter pressure environment is implemented

* Corresponding author. Tel.: +7 903 247 9742.
E-mail addresses: immras@orc.ru (M.G. Lobok), b.chichkov@lhz.de (B. Chichkov).

0169-4332/$ – see front matter © 2008 Elsevier B.V. All rights reserved.
doi:10.1016/j.apsusc.2008.08.014

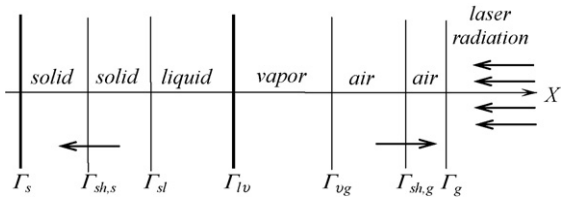

Fig. 1. Spatial distribution of phase states and shockwaves.

within one-dimensional multiphase hydrodynamic Stephan problem equated for both of liquid and solid phase:

$$\left[\begin{array}{l}
\dfrac{\partial\rho}{\partial t}+\dfrac{\partial(\rho u)}{\partial x}=0,\\
\dfrac{\partial(\rho u)}{\partial t}+\dfrac{\partial(\rho u^2)}{\partial x}+\dfrac{\partial P}{\partial x}=0,\\
\dfrac{\partial(\rho\varepsilon)}{\partial t}+\dfrac{\partial(\rho u\varepsilon)}{\partial x}=-\left(P\dfrac{\partial u}{\partial x}+\dfrac{\partial W_{\mathrm{T}}}{\partial x}+\dfrac{\partial W_{\mathrm{l}}}{\partial x}+\dfrac{\partial G}{\partial x}\right),\\
\dfrac{\partial I_\upsilon}{\partial x}+\kappa(h\nu,\rho,T)I_\upsilon=\kappa(h\nu,\rho,T)I_{\mathrm{v,eq}},\\
W_\upsilon=\displaystyle\int_0^\infty\int_{-1}^1\mu I_\upsilon\,\mathrm{d}\nu\,\mathrm{d}\mu,\quad W_{\mathrm{T}}=-\lambda(T)\dfrac{\partial T}{\partial x},\\
\dfrac{\partial G}{\partial x}-\kappa_{\mathrm{L}}(\rho,T)G=0,\\
P=P(\rho,T),\quad \varepsilon=\varepsilon(\rho,T)
\end{array}\right]_k,\ k$$
$$=\mathrm{s},\ \mathrm{l},\ \upsilon,\ \mathrm{g} \tag{1}$$

$$x\in[\Gamma_{\mathrm{s}},\ \Gamma_{\mathrm{sh,s}}]\cup[\Gamma_{\mathrm{sh,s}},\ \Gamma_{\mathrm{sl}}]\cup[\Gamma_{\mathrm{sl}},\ \Gamma_{\mathrm{lv}}]\cup[\Gamma_{\mathrm{lv}},\Gamma_{\mathrm{ug}}]\cup[\Gamma_{\mathrm{ug}},\Gamma_{\mathrm{sh,g}}]\cup[\Gamma_{\mathrm{sh,g}},\Gamma_{\mathrm{g}}]$$

Stephan problem is conjugated with system of equations of radiative thermodynamics with thermoconductivity, which describes processes in the evaporated material and surrounding gas.

Where ρ, u, ε, T and P stand for density, gas dynamical velocity, internal energy, temperature and pressure, respectively, κ and I_ν are the coefficient of absorption and spectral density of plasma irradiation, $I_{\nu,\mathrm{eq}}$ is the equilibrium irradiation density, κ_{L} and G are the coefficients of absorption and intensity of laser irradiation, λ is the thermoconductivity coefficient. Indexes s, l, v and g are for description of different phases: solid, liquid, vapor and gas.

2.1. Boundary conditions

1. For left non-moving boundary we set $x=\Gamma_{\mathrm{sl}}$:
$$u=0,\quad W_{\mathrm{T}}=0,\quad W_{\mathrm{l}}=0 \tag{2}$$
2. For melting/crystallization front $x=\Gamma_{\mathrm{sl}}$: there are three laws of conservation formulated on this boundary: mass, momentum and energy, written in the system which moves with the velocity of the melting front $\upsilon_{\mathrm{sl}}=\upsilon^*_{\mathrm{sl}}-u_{\mathrm{s}}$, where υ^*_{sl} is velocity of the melting (crystallization) in non-moving coordinate system:
$$\rho_{\mathrm{s}}\upsilon_{\mathrm{sl}}=\rho_{\mathrm{l}}(u_{\mathrm{l}}-u_{\mathrm{s}}-\upsilon_{\mathrm{sl}}) \tag{3}$$
$$P_{\mathrm{s}}+\rho_{\mathrm{s}}\upsilon_{\mathrm{sl}}^2=p_{\mathrm{l}}+\rho_{\mathrm{l}}(u_{\mathrm{l}}-u_{\mathrm{s}}-\upsilon_{\mathrm{sl}})^2 \tag{4}$$
$$W_{\mathrm{l}}^{\mathrm{T}}-W_{\mathrm{s}}^{\mathrm{T}}=\rho_{\mathrm{s}}\upsilon_{\mathrm{sl}}L_{\mathrm{m}}^{\mathrm{ne}} \tag{5}$$

where $W_{\mathrm{s}}=-\lambda(T_{\mathrm{s}})(\partial T_{\mathrm{s}}/\partial x)$, $W_{\mathrm{l}}=-\lambda(T_{\mathrm{l}})(\partial T_{\mathrm{l}}/\partial x)$ and C_{ps}, $C_{p\mathrm{l}}$ thermal capacity of solid and liquid states, respectively:

$$L_{\mathrm{m}}^{\mathrm{ne}}=L_{\mathrm{m}}+(C_{p\mathrm{l}}-C_{ps})(T_{\mathrm{sl}}-T_{\mathrm{m}})+\frac{\rho_{\mathrm{s}}+\rho_{\mathrm{l}}}{\rho_{\mathrm{s}}-\rho_{\mathrm{l}}}\frac{(u_{\mathrm{s}}-u_{\mathrm{l}})^2}{2}$$

is non-equilibrium melting heat. Law of energy conservation (5), representing differential Stephan condition is supplemented with phenomenological condition of temperatures equality:

$$T_{\mathrm{sl}}=T_{\mathrm{s}}=T_{\mathrm{l}}=T_{\mathrm{m}}(P_{\mathrm{s}}) \tag{6}$$

Melting temperature T_{m} is supposed to be dependent on the pressure $T_{\mathrm{m}}(P_{\mathrm{s}})$.

Evaporation $x=\Gamma_{\mathrm{v}}$: three conservation laws are formulated in the system of coordinates moving with velocity the melting front on the evaporating surface $\upsilon_{\mathrm{sl}}=\upsilon^*_{\mathrm{sl}}-u_{\mathrm{s}}$:

$$\rho_{\mathrm{l}}\upsilon_{\mathrm{lv}}=\rho_\upsilon(u_{\mathrm{l}}-u_\upsilon+\upsilon_{\mathrm{lv}}) \tag{7}$$
$$P_{\mathrm{l}}+\rho_{\mathrm{l}}\upsilon_{\mathrm{l}}^2=p_\upsilon+\rho_\upsilon(u_{\mathrm{l}}-u_\upsilon+\upsilon_{\mathrm{lv}})^2 \tag{8}$$
$$W_{\mathrm{l}}^{\mathrm{T}}-W_\upsilon^{\mathrm{T}}=-\rho_{\mathrm{l}}\upsilon_{\mathrm{lv}}L_\upsilon^{\mathrm{ne}},\quad G=A(T)G_{\mathrm{l}},\quad W_\upsilon=W_\upsilon^{\mathrm{l}} \tag{9}$$

where

$$L_\upsilon^{\mathrm{ne}}=L_\upsilon^{\mathrm{e}}(T_{\mathrm{l}})+C_{p\upsilon}(T_{\mathrm{b}}-T_{\mathrm{lv}})+\frac{\rho_{\mathrm{l}}+\rho_\upsilon}{\rho_{\mathrm{l}}-\rho_\upsilon}\frac{(u_{\mathrm{l}}-u_\upsilon)^2}{2}$$

is non-equilibrium latent evaporation heat, T_{b} boiling temperature. T_{v}, ρ_{v} and p_{v} are found from correspondence on non-equilibrium Knudsen layer, using Crout modified model [18]: $T_{\mathrm{v}}=\alpha T(M)T_{\mathrm{l}}$, $\rho_{\mathrm{v}}=\rho_{\mathrm{H}}\alpha_\rho(M)$, where $\alpha_{\mathrm{T}}(M)$, $\alpha_\rho(M)$, Crout coefficients; $M=u_{\mathrm{v}}/u_{\mathrm{sh}}$, vapor velocity in Mach numbers and

$$\rho_{\mathrm{H}}=\frac{P_{\mathrm{H}}(T_{\mathrm{l}})}{R_\mu T_{\mathrm{l}}},\quad P_{\mathrm{H}}(T_{\mathrm{l}})=P_{\mathrm{b}}\exp\left[\left(\frac{1}{T_{\mathrm{b}}}-\frac{1}{T_{\mathrm{l}}}\right)\frac{L_\upsilon}{R_\mu}\right]$$

density and saturated pressure for vapor at temperature T_{l}.

An aluminum target ~30 μm thick situated in the air medium at a temperature of $T_0=273$ K and under pressure of $P_0=10^5$ Pa was examined. The corresponding thermophysical parameters were chosen for solid and liquid aluminum states. Equilibrium melting temperature is $T_{\mathrm{m},0}=933$ K. As a function $T_{\mathrm{m}}(P_{\mathrm{s}})$ was accepted an experimental dependence [19] approximated with relationship $T_{\mathrm{m}}(P_{\mathrm{s}})=(T_{\mathrm{m},0}+kP_{\mathrm{s}})$, where $k=\partial T_{\mathrm{m}}/\partial P_{\mathrm{s}}=2\times10^{-9}$ K/Pa. Critical temperature for aluminum was assumed as $T_{\mathrm{cr}}=8\times10^3$ K [20]. Starting from the temperature value of $T=0.85T_{\mathrm{cr}}$, subject to heat conductivity and laser radiation absorption factors were exponentially reducing and heat capacity rate was exponentially increasing till the critical point value $\lambda_{\mathrm{cr}}=0.01$ J/(K cm), $\kappa_{\mathrm{cr}}=10^3$ cm^{-1} and $C_{\mathrm{cr}}=10.200$ J s/(g K). Wide-range equation of state was used [21].

3. Calculation algorithm

Numerical solution of the differential problem (1)–(9) was provided using finite difference method with dynamic adaptation [22] allowing to do computations with direct tracking of interphase boundaries and shockwaves. As the result we can have up to six areas for computation with seven boundaries, six of them being moving boundaries, including two shockwaves and right free boundary in the air.

4. Results

The above-mentioned model (1)–(9) was used for modeling several regimes, in which solid aluminum target is irradiated by Gaussian time profile laser pulse with duration $\tau=10^{-15}$ to 10^{-12} s and peak intensity $G_0=10^{12}$ to 10^{16} W/cm^2. In this distribution time moment $t=0$ corresponds to peak intensity, and calculation starts at $t=-4\tau$. For all calculations $J=G_0\tau$ was constant and equal to 10 J/cm^2, absorption coefficient of the target $A=10\%$. Modeling revealed that, plasma in the evaporated material is formed for J higher than 10 J/cm^2, due to the fact that plasma slows the process of evaporation, the most attention was paid to the regimes prior to plasma formation.

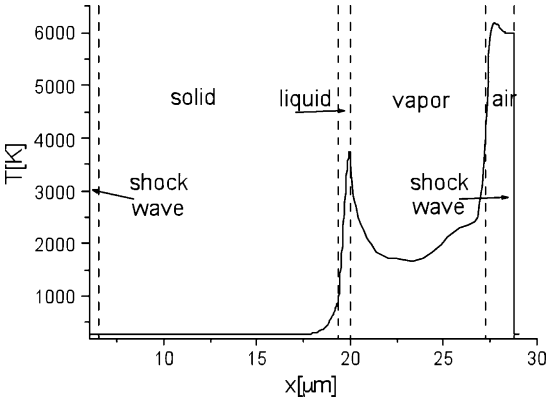

Fig. 2. Spatial profile of temperature at $t = 2.5$ ns for pulse duration $\tau = 1$ ps and intensity $G_0 = 10^{13}$ W/cm^2.

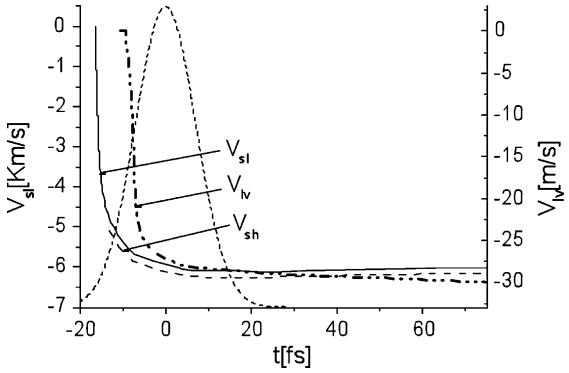

Fig. 4. Temporal profiles for velocities of melting, evaporation, and shockwave in for pulse duration $\tau = 10$ fs and intensity $G_0 = 10^{15}$ W/cm^2.

Part of the processes taking place in condensed environment has general character non-depending on pulse duration (Figs. 2 and 3). In our case we have volumetric energy absorption in condensed state. Heating of the target surface up to equilibrium melting temperature $T_{m,0}$ leads to creation of liquid phase with initial thickness of about 0.2–0.5 nm. Volumetric mechanism of heat absorption and matter flux though interphase boundary $x = \Gamma_{sl}$ are forming in solid phase an undersurface temperature maximum. Spatial position of this maximum is defined by correspondence between temperature conductivity, absorption coefficient and melting front velocity [13,14]. At the moment then saturated vapor pressure excides air pressure starts the convective evaporation from the surface. Affected by quickly evaporating liquid, another undersurface temperature maximum is formed at a distance from the evaporation front (Fig. 3) and in the gas medium, a powerful vapor flux is formed with gas dynamical velocity reaching 3 km/s. The rapidly expanding vapor works as an accelerating piston pushing out cold air, which creates a shockwave in the gas medium (Figs. 2 and 3). The shockwave, identified using Rankin–Gugonio conditions, propagates towards laser radiation. Indicated features are typical for both pico- and femtosecond laser pulses. However, the dynamics of the phase shifts has its own particularities.

4.1. Melting

Melting front dynamic strongly depends on laser pulse duration. As it follows from auto-model solution [23] at $t \to 0$ velocity of melting is $\upsilon_{sl} \to \infty$. Thus, υ_{sl} would increase with decreasing of laser pulse duration. In reality, velocity of melting always stays a finite value, even for a metastable solid. One of the effective mechanisms of υ_{sl} limiting is hydrodynamics of the melted matter. Its influence affects in particular depending on melting temperature T_m, pressure on melting surface P_s: $T_m = T_m(P_s)$ (Fig. 4).

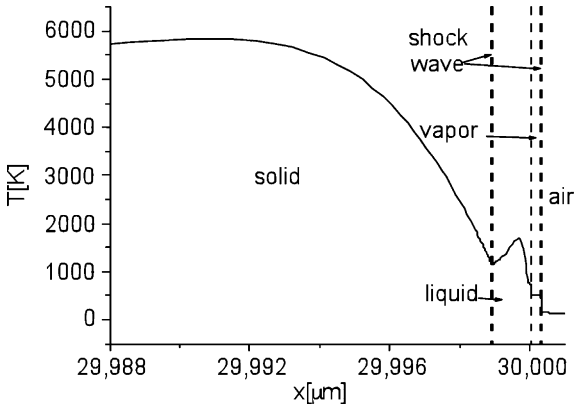

Fig. 3. Spatial profile of temperature at $t = 78.5$ fs for pulse duration $\tau = 10$ fs and intensity $G_0 = 10^{15}$ W/cm^2.

During long-time pulses $\tau > 10^{-9}$ s and energy density <10 J/cm^2, melting process runs ordinary. Maximum melting velocity reaches a few hundred meters per second, and pressure $P_s < 4 \times 10^8$ Pa. Temperature on interphase boundary $T_{sl} \cong T_m$ does not almost differ from equilibrium melting temperature T_m. Temperature maximum is in some distance from interphase boundary and exceeds equilibrium melting temperature for several tens degrees. Such solid phase slight overheating quickly disappears, without any significant effect on the melting process.

Decrease of pulse duration is accompanied by growth of the heating velocity, and accordingly melting velocity υ_{sl}. Increase of melting velocity leads to both pressure P_s and melting temperature $T_m = T_m(P_s)$ increase. In picosecond diapason near ablation barrier $J > 0.1$ J/cm^2 evaporation role is insignificant. The main feature of such regimes is that the thickness of liquid phase does not exceed 10–20 nm, and that makes it transparent for laser irradiation. Energy of the laser pulse is almost completely absorbed by solid phase, causing its significant overheating ($T_{max} \sim 2000$ K). Stored energy is spent on heating and melting of the solid phase. That is why at low $J < 1$ J/cm^2 process of melting is efficient. To strength ablation during picosecond laser pulse, energy density should be above 1 J/cm^2.

For laser pulses shorter than $\tau = 10^{-12}$ s and $J > 1$ J/cm^2 melting velocity growth is limited to sonic velocity in solid matter, which is about 6260 m/s for aluminum. As velocity of melting approaching sonic velocity creates, on the one hand conditions for shockwave appearance in solid phase, and on the other hand for peak overheating to T_{max} about 7000 K. In picosecond's diapason melting velocity front lies between 4000 and 6000 m/s, and temperature $T_{sl} \gg T_{m,0} \approx (2.5–6) \times 10^3$ K and pressure $P_s = (0.1–1) \times 10^{11}$ Pa. This pressure is enough to create a strong shockwave in solid phase. Afterwards, the melting front and the shockwave expand together as single complex. In femtosecond diapason overheating parameters are as follows: $\upsilon_{sl} \cong 5000–6260$ m/s, $T_{sl} \gg T_{m,0} \approx (5.5–7.8) \times 10^3$ K, $T_{max} = 8000$ K and $P_s = (1–2) \times 10^{11}$ Pa.

Some time after the end of the pulse (about 10^{-10} s) temperature gradients difference close to phase front of melting velocity significantly reducing, which first of all affects melting front velocity, which drops to several tens meters per second and left behind the shockwave. The shockwave becomes decaying and continue moving getting far from interphase boundary with

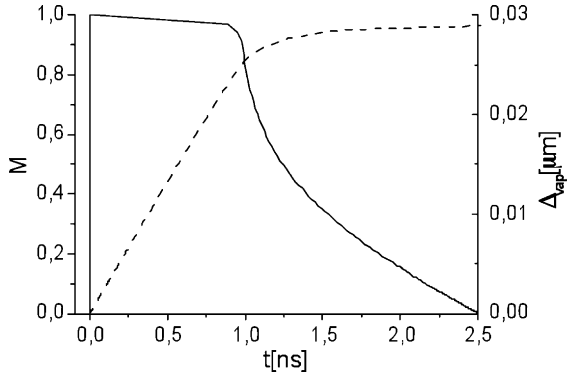

Fig. 5. Time profile of evaporation velocity in Mach numbers and thickness of evaporated layer for pulse duration $\tau = 1$ ps and intensity $G_0 = 10^{13}$ W/cm^2.

decreasing intensity, because of the pressure drop from 10^{11} to 10^9 Pa at the same time being ahead of shockwave.

4.2. Evaporation

Within pico- and femtosecond range with $J > 1$ J/cm^2 target fast heating, high melting velocity and slow energy transfer at the expense of heat conductivity lead to considerably greater overheating of the solid phase than in case of long pulses. Peak temperature inside of solid matter is at the depth of ~0.02 μm from Γ_{sl} and makes about 6000 to 8000 K. During pulse action the small amount of liquid appears. Liquid phase thickness does not exceed the value of 30 nm during pulse action. Due to clearance in around critical area it is almost transparent for laser irradiation. As the result we have almost constant temperature $T_{sl} = T_{lv}$ in liquid. After the end of the pulse action the saved energy of the overheated solid phase is spent for heating of liquid phase and maintaining high temperature on the surface. This provides much longer evaporation time than pulse duration (Fig. 5). Since energy transfer from overheated solid fuel field to liquid phase is implemented by relatively slow mechanism of thermoconductivity, evaporation time is almost the same for pico- and femtosecond laser pulse and is about 2.5–3 ns. Overheated metastable states completely disappear when t is about 1 ns.

State of the vapor near evaporation surface in prior to plasmatic regime is mainly defined by the temperature on the vaporizing surface and liquid thermoconductivity. Vapor heating at the expense of absorption of laser irradiation for which it is almost transparent is insignificant. Thickness of the vapor field during laser pulse is rather small and is just about 7 nm, and by the end of evaporation process it reaches value of 7.5 μm (Fig. 2). Thickness of the evaporated layer is about 0.29 nm (Fig. 5). If the intensity is high enough, avalanche growth of temperature, concentration of charged particles and absorption coefficient near evaporation surface begins. This process of high ionized and absorbing plasma formation is equilibrium analog of optical breakthrough. Vapor temperature rises up to 10^6 K fast, electron concentration $N_e \approx 8 \times 10^{22}$ cm^{-3} and absorption coefficient $\kappa \approx 10^5$ cm^{-1}. A shockwave appears which expands in direction from the surface reaches the first shockwave in gas and absorbs it. Decrease of laser irradiation on the surface of the target caused by growth of pressure in plasma leads elimination of surface evaporation.

5. Conclusion

Volumetric dissipation mechanism, inherent to short pulse interaction, leads to qualitative changes of the basic processes in irradiated area. These changes are defined by appearance of metastable states, related to liquid and solid undersurface layers overheating. Overheating of both phases is interrelated with phase transformations. Maximum overheating reaches six to eight times value of equilibrium melting temperature. Phase transitions times weakly depends on laser pulse duration, and they several orders of magnitude longer. Evaporated depth for intensity $G = 10^{12}$ W/cm^2 is 10–20 nm, and molten pool does not exceed 10 nm, which corresponds to experimental data [2]. At our assumptions lifetimes of metastable states are nanoseconds after pico- or femtosecond laser pulse. One of the main metastable state features is its limited lifetime. During laser impact on condensed environments those problems are coming to definition of relative role of surface and volumetric mechanism of melting and evaporation. In mathematical model considered in this research it is assumed that overheated metastable states behave steadily and surface melting and evaporation processes are the main mechanism of phase transformation: solid–liquid and liquid–vapor. Thereby nucleation processes and related to it volumetric melting and evaporation processes are out of the consideration. It allows to considerably simplify the problem formulation otherwise the metastable phase's explosive disintegration should be taken into consideration. At the present time theoretical models on the basis of which the quantitative analysis could be conducted do not exist.

Acknowledgments

This study was partly supported by RFBR grant nos. 07-07-00045-a and DFG-08-07-91950.

References

[1] J.C. Miller (Ed.), Laser Ablation. Principles and Applications, Springer, Berlin, 1994, p. 185.
[2] M.D. Shirk, P.A. Molian, J. Laser Appl. 10 (1998) 18.
[3] K. Sokolowski-Tinten, D. von der Linde, Phys. Rev. B 61 (2000) 2643.
[4] V.M. Gordienko, M.S. Dzhidzhoev, V.V. Kolchin, et al. Kvantovaya electronika (Russian) 22 (1995) 158.
[5] E.G. Gamaly, A.V. Rode, V.T. Tikhonchuk, et al. Phys. Plasmas 9 (2002) 949.
[6] L.V. Zhigilei, D. Ivanov, E. Leveugle, Proc. SPIE 5448 (2004) 505.
[7] Zh. Lin, L.V. Zhigilei, Proc. SPIE 6261 (2006), 62610U-1.
[8] X. Xu, C. Grigoropoulos, R.E. Russo, Appl. Phys. Lett. 65 (1994) 1745.
[9] S. Williamson, C. Mourou, J.C.H. Li, Phys. Rev. Lett. 52 (1984) 2364.
[10] G.I. Alferov, Yu.V. Kovalchuk, Yu.V. Pogorelsky, O.V. Smolsky, Izvestiya AN SSSR, Seriya fizicheskaya 49 (1985) 1069.
[11] M. Kandyla, T. Shih, E. Mazur, Phys. Rev. B 75 (2007) 214107.
[12] A. Peterlongo, A. Miotello, R. Kelly, Phys. Rev. E 50 (1994) 4716.
[13] V.I. Mazhukin, I. Smurov, C. Dupuy, et al. J. Numer. Heat Transfer, Part A 26 (1994) 587.
[14] V.I. Mazhukin, I. Smurov, G. Flamant, J. Appl. Phys. 78 (1995) 1259.
[15] E.G. Gamaly, EMRS-2008, Book of Abstract, Strasburg, 2008.
[16] D. Ivanov, L.V. Zhigilei, Phys. Rev. B 68 (2003) 064114–064121.
[17] D. Ivanov, L.V. Zhigilei, Phys. Rev. Lett. 98 (2007) 195701–195711.
[18] V.I. Mazhukin, P.A. Prudkovskii, A.A. Samokhin, Matematicheskoe modelirovanie (Russian) 5 (1993) 3.
[19] J. Lees, B.H.J. Williamson, Nature 208 (1965) T84.
[20] V.E. Fortov, A.N. Dremin, A.A. Leont'ev, Teplofizika vysokih temperature (Russian) 13 (1975) 176.
[21] K.S. Holian, J. Appl. Phys. 59 (1986) 149.
[22] P.V. Breslavsky, V.I. Mazhukin, Comput. Math. Math. Phys. 47 (2007) 687.
[23] H.S. Carslaw, J.C. Jaeger, Conduction of Heat in Solids, Clarendon Press, Oxford, 1959, p. 510.